Fidelity in Hapten Design: How Analogous Are Phosphonate Haptens to the Transition States for Alkaline Hydrolyses of Aryl Esters?

Dean J. Tantillo and K. N. Houk*

Department of Chemistry and Biochemistry, University of California, Los Angeles, 405 Hilgard Avenue, Los Angeles, California 90095-1569

Received November 30, 1998

Is antibody catalysis of hydrolysis reactions limited by imperfect mimicry of transition states by haptenic analogs? This question was explored by comparison of calculated transition states for the hydrolyses of aryl esters and the haptens intended to mimic them. The addition−elimination reaction of phenyl acetate and hydroxide ion in the gas phase was examined using ab initio calculations at the RHF/6-31+G(d)//RHF/6-31+G(d) and MP2/6-31+G(d)//RHF/6-31+G(d) levels of theory. Although transition states for both addition and elimination were located, the barrier to elimination disappeared when zero point energy or electron correlation was included. The reaction is therefore concerted, and the transition state for addition is the only relevant transition state in the gas phase. When aqueous solvation is considered through PCM and SCI-PCM calculations, the barrier to addition is shown to increase dramatically, and a stepwise addition−elimination pathway is predicted. A single transition state for the analogous reaction with *p*-nitrophenyl acetate was also located, and this reaction is predicted to be concerted in both the gas phase and in solution. The calculated geometries, CHELPG atomic charges, and electrostatic potential surfaces of stationary points involved in hydrolysis were compared with those of model phosphonate and phosphinate haptens. The haptens are better mimics of the two transition states and the tetrahedral intermediate than of the reactants or products—exactly the situation desired for catalyst generation—yet they are more analogous to the tetrahedral intermediate and the transition state for elimination than to the rate-determining addition transition state. In addition, the hydrogen-bonding pattern and asymmetry of the stationary points are not faithfully reproduced by the haptens. These considerations suggest that catalysis may be improved by hapten redesign or antibody mutagenesis.

Introduction

Antibody catalysis of organic reactions has provided a new means to harness Nature's combinatorial prowess for synthetic and therapeutic applications. Promising successes and unrealized expectations have marked the intense activity in this field over the past decade.[1] Immune responses to antigens (haptens) which resemble the putative transition states of many different reactions have produced antibodies which bind those transition states and consequently provide catalysis. Many antibodies capable of catalyzing both biological and nonbiological reactions have been developed, but few have reached the levels of efficiency characteristic of enzymes. Some antibody catalysts function with high selectivity, yet others are rather promiscuous. A recent review has provided a thoughtful examination of the strengths and weaknesses of the transition state analog (TSA) strategy for catalyst generation,[2] but detailed explanations of interactions between antibodies and their haptens are limited to the small fraction of catalysts whose structures have been solved by X-ray crystallography. The key to catalysis is, however, the nature of the specific interactions involved in transition state binding by the antibody combining site. As a first step toward achieving understanding of antibody catalysis at the molecular level, we have examined the fidelity with which several specific haptens mimic the geometries and electrostatic properties of transition states and intermediates involved in an antibody-catalyzed reaction.

We have studied the alkaline hydrolysis of aryl acetate derivatives. The majority of antibody-catalyzed reactions have been aryl ester and amide hydrolyses.[1a,b] Such reactions are not only of interest in the catalytic antibody field but have also found application in many other disciplines such as physical organic,[3] biological,[4] bioinorganic,[5] polymer[6] and supramolecular chemistry.[7] In particular, *p*-nitrophenyl esters have been used in nu-

(1) Recent reviews include the following: (a) Thomas, N. R. *Nat. Prod. Rep.* **1996**, 479−511. (b) Lerner, R. A.; Benkovic, S. J.; Schultz, P. G. *Science* **1991**, *252*, 659−667. (c) Schultz, P. G.; Lerner, R. A. *Science* **1995**, *269*, 1835−1842. (d) Stewart, J. D.; Liotta, L. J.; Benkovic, S. J. *Acc. Chem. Res.* **1993**, *26*, 396−404. (e) Smithrud, D. B.; Benkovic, S. J. *Curr. Opinion Biotech.* **1997**, *8*, 459−466. (f) Kirby, A. *Acta Chem. Scand.* **1996**, *50*, 203-210. (g) Hiratake, J.; Oda, J. *J. Synth. Org. Chem. Jpn.* **1997**, *55*, 452−459.

(2) Mader, M. M.; Bartlett, P. A. *Chem. Rev.* **1997**, *97*, 1281−1301.

(3) Recent examples include the following: (a) Hengge, A. C.; Hess, R. A. *J. Am. Chem. Soc.* **1994**, *116*, 11256−11263. (b) Stefanidis, D.; Cho, S.; Dhe-Paganon, S.; Jencks, W. P. *J. Am. Chem. Soc.* **1993**, *115*, 1650−1656. (c) Um, I.-H.; Lee, G.-J.; Yoon, H.-W.; Kwon, D.-S. *Tetrahedron Lett.* **1992**, *33*, 2023−2026. (d) Marsh, M. R.; Gold, V.; Hall, C. D.; Sghibartz, C. *J. Chem. Res., Synop.* **1989**, 248−249. (e) Ba−Saif, S.; Luthra, A. K.; Williams, A. *J. Am. Chem. Soc.* **1989**, *111*, 2647−2652. (f) Buncel, E.; Um, I. H.; Hoz, S. *J. Am. Chem. Soc.* **1989**, *111*, 971−975. (g) Ba−Saif, S.; Luthra, A. K.; Williams, A. *J. Am. Chem. Soc.* **1987**, *109*, 6362−6368. (h) Hess, R. A.; Hengge, A. C.; Cleland, W. W. *J. Am. Chem. Soc.* **1998**, *120*, 2703−2709.

(4) Recent examples include the following: (a) Broo, K. S.; Brive, L.; Ahlberg, P.; Baltzer, L. *J. Am. Chem. Soc.* **1997**, *119*, 11362−11372. (b) Anderson, J.; Byrne, T.; Woelfel, K. J.; Meany, J. E.; Spyridis, G. T.; Pocker, Y. *J. Chem. Educ.* **1994**, *71*, 715−718. (c) Roa, A.; Goble, M. L.; Garcia, J. L.; Acebal, C.; Virden, R. *Biochem. J.* **1996**, *316*, 409−412. (d) Rahil, J.; Pratt, R. F. *Biochemistry* **1994**, *33*, 116−125.

10.1021/jo982335t CCC: $18.00
Published on Web 04/02/1999

Scheme 1

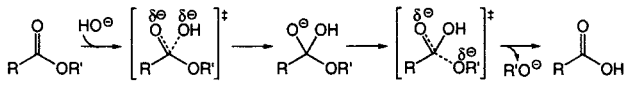

Chart 1

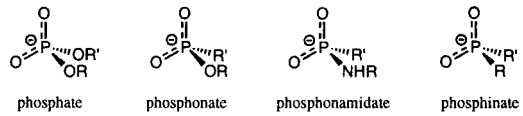

merous physical organic and biochemical studies due to the ease of detecting the *p*-nitrophenoxide anion produced in base-catalyzed hydrolysis.[4b] In fact, their repeated use has even been described by one author as the "*p*-nitrophenyl ester syndrome".[8]

The accepted mechanism for base-promoted ester hydrolysis is shown in Scheme 1. This mechanism involves a high-energy anionic tetrahedral intermediate flanked by two charge-delocalized anionic transition states; all three are assumed to have rather similar structures. Haptens designed to mimic the tetrahedral intermediate and the two transition states have been used to elicit antibodies which catalyze the hydrolysis of certain esters, amides, carbonates, and carbamates, as well as some which catalyze transesterification and ester aminolysis reactions.[1a,b] These haptens are normally phosphates, phosphonates, phosphonamidates, and phosphinates and their esters (Chart 1), which are expected to mimic the charge-delocalization and tetrahedral geometry of the transition states. While transition states can share recognition elements with ground state molecules, it is obvious that transition state analogs can never represent geometries and charge distributions of transition states exactly. We have examined the transition states involved in the hydrolyses of phenyl and *p*-nitrophenyl acetate and have compared them with haptens designed according to the TSA strategy. Despite some similarities, we find significant deviations in hapten structure from transition state geometries and electrostatic properties. The implications of this imperfect mimicry for antibody catalysis of ester hydrolyses are discussed.

Methods

All ab initio calculations were performed with the GAUSSIAN 94 program.[9] All stationary point geometries were optimized at the RHF/6-31+G(d) level unless otherwise noted, while reported energies are from calculations on these geometries carried out at the RHF/6-31+G(d) or MP2/6-31+G(d) level. A basis set with diffuse functions was used because of the anionic nature of the species involved in this reaction. In addition, all stationary points were characterized by frequency calculations at the RHF/6-31+G(d) level, and zero point energy corrections (scaled by 0.9153)[10] from these calculations are included in the reported energies. All transition states were further characterized by analysis of the normal modes corresponding to their imaginary frequencies and, in some cases, by intrinsic reaction coordinate (IRC) calculations (as described below).

Polarized continuum model (PCM)[11] and self-consistent isodensity PCM (SCI-PCM)[12] self-consistent reaction field (SCRF) single point calculations at the RHF/6-31+G(d) level were performed on selected stationary points to address solvation effects. Both models utilized a dielectric constant of 78.5 in order to simulate an aqueous environment, and PCM calculations were performed with 100 points per overlapping sphere. Reported energies include zero point energy corrections from the RHF/6-31+G(d) frequency calculations described above. Such methods model the solvent as a continuum of uniform dielectric and therefore do not take into account explicit solvent−solute interactions such as hydrogen bonding. However, it has recently been reported that SCI-PCM single point calculations on gas phase ab initio geometries of stationary points involved in the addition of hydroxide ion to *N*,*N*-dimethylacetamide underestimate absolute aqueous solvation enthalpies but accurately reproduce experimental activation barriers.[12c] Only minor changes to structures and energetics were observed when geometries were fully optimized in the presence of a continuum solvent model.[12c]

To facilitate comparisons of hapten and transition state structures, hapten geometries were also optimized at the RHF/6-31+G(d) level, using coordinates from the antibody-bound structures as starting geometries.[13−15] This provided a consistent set of bond lengths and angles, whereas the magnitude of these quantities varied considerably in the different antibody-bound X-ray structures. These structures were each determined to a resolution of ≥ 2 Å (with crystallographic *R* factors of ≥ 0.18), and as a result, some of the reported P−O bond lengths in these structures deviate significantly from expectations (based on a survey of bond lengths observed in X-ray and neutron diffraction studies of small molecules, all with *R* factors ≤ 0.07).[16] Energies were calculated for each optimized structure at the RHF/6-31+G(d) and MP2/6-31+G(d) levels. Torsional angles were constrained in most hapten optimizations, since these structural parameters can be strongly influenced by the surrounding protein environment. Relaxation of bond lengths and angles was allowed, however, and reduced the energy of the 48G7 hapten by approximately 70−90 kcal/mol, the CNJ206 hapten by approximately 40 kcal/mol, and the 17E8 hapten by approximately 5 kcal/mol relative to the energies of the hapten structures extracted from the hapten−antibody complexes. Most changes in energy were due to adjustments in P−O bond lengths, which relaxed to values consistent with those observed in related unbound molecules.[16] Although slight changes to bond lengths and angles may be induced by the antibody combining sites, changes of the magnitude observed for the 48G7 and CNJ206 haptens are likely not protein-induced. The structure of a theoretical phosphinate TSA was also fully optimized at the RHF/6-31+G(d) level using the relaxed 17E8 hapten structure, with the ether oxygen atom replaced by a methylene group, as a starting geometry.

(5) Yatsimirsky, A. K.; Diky, A. I. *Inorg. Chim. Acta* **1991**, *186*, 161−163.
(6) Wang, G.-J.; Fife, W. K. *J. Am. Chem. Soc.* **1998**, *120*, 883−887.
(7) Gadosy, T. A.; Tee, O. S. *Can. J. Chem.* **1996**, *74*, 745−752.
(8) Menger, F. M.; Ladika, M. *J. Am. Chem. Soc.* **1987**, *109*, 3145−3146.
(9) Frisch, M. J.; Trucks, G. W.; Schlegel, H. B.; Gill, P. M. W.; Johnson, B. G.; Robb, M. A.; Cheeseman, J. R.; Keith, T.; Petersson, G. A.; Montgomery, J. A.; Raghavachari, K.; Al-Laham, M. A.; Zakrzewski, V. G.; Ortiz, J. V.; Foresman, J. B.; Cioslowski, J.; Stefanov, B. B.; Nanayakkara, A.; Challacombe, M.; Peng, C. Y.; Ayala, P. Y.; Chen, W.; Wong, M. W.; Andres, J. L.; Repogle, E. S.; Gomperts, R.; Martin, R. L.; Fox, D. J.; Binkley, J. S.; Defrees, D. J.; Baker, J.; Stewart, J. P.; Head-Gordon, M.; Gonzales, C.; Pople, J. A. *Gaussian 94*; Gaussian, Inc.: Pittsburgh, PA, 1995.
(10) Scott, A. P.; Radom, L. *J. Phys. Chem.* **1996**, *100*, 16502−16513.
(11) (a) Miertus, S.; Tomasi, J. *Chem. Phys.* **1982**, *65*, 239−245. (b) Miertus, S.; Scrocco, E.; Tomasi, J. *Chem. Phys.* **1981**, *55*, 117−129.
(12) (a) Wiberg, K. B.; Keith, T. A.; Frisch, M. J.; Murcko, M. *J. Phys. Chem.* **1995**, *99*, 9072−9079. (b) Wiberg, K. B.; Castejon, H. *J. Comput. Chem.* **1996**, *17*, 185−190. (c) Zheng, Y.-J.; Ornstein, R. L. *J. Mol. Struct. (THEOCHEM)* **1998**, *429*, 41−48.
(13) Wedemayer, G. J.; Wang, L. H.; Patten, P. A.; Schultz, P. G.; Stevens, R. C. *J. Mol. Biol.* **1997**, *268*, 390−400.
(14) Golinelli-Pimpaneau, B.; Gigant, B.; Bizebard, T.; Navaza, J.; Saludjian, P.; Zemel, R.; Tawfik, D. S.; Eshhar, Z.; Green, B. S.; Knossow, M. *Structure* **1994**, *2*, 175−183.
(15) Zhou, G. W.; Guo, J. C.; Huang, W.; Fletterick, R. J.; Scanlan, T. S. *Science* **1994**, *265*, 1059−1064.
(16) Allen, F. H.; Kennard, O.; Watson, D. G.; Brammer, L.; Orpen, A. G.; Taylor, R. *J. Chem. Soc., Perkin Trans. 2* **1987**, S1−S19.

Table 1. Relative Enthalpies (kcal/mol) of RHF/6-31+G(d) Stationary Points Involved in Phenyl Acetate Hydrolysis[a]

level of theory	1 + 2	3	4	5	6	7	8 + 9	10 + 11	12	13	14
RHF/6-31+G(d)	54.0	34.2	0.0	−12.9	−14.5	−19.0	6.4	3.6	17.9	37.5	17.6
MP2/6-31+G(d)	50.9	26.5	0.0	−13.5	−20.2	−18.9	10.6	7.9	9.5	27.0	8.2
RHF/6-31+G(d)/PCM	7.6	20.7	0.0			−17.9	−8.6	−12.4	12.1	26.4	13.8
RHF/6-31+G(d)/SCI-PCM	21.4	27.6	0.0			−20.7	−5.8	−17.9	15.3	31.5	16.4

[a] All energies include the zero point energy correction calculated at the RHF/6-31+G(d) level of theory.

Table 2. Entropy Corrections ($-T\Delta S$ at 298 K, kcal/mol) to the Free Energies of RHF/6-31+G(d) Stationary Points Involved in Phenyl Acetate Hydrolysis

1 + 2	3	4	5	6	7	8 + 9	10 + 11	12	13	14
−36.9	−32.0	−34.0	−33.9	−33.0	−34.0	−42.0	−43.4	−30.0	−29.8	−29.8

Molecular volumes were calculated and compared using the Molecular Shape Analysis function accessible through the Superposition Module in SPARTAN.[17] For all molecular volume calculations, optimized bond lengths and angles were used, the Ph−O−C(P)−Me dihedral angle in each structure was fixed at 180°, and the dihedral angle about the Ph−O bond was fixed at 90°. The truncated 17E8 hapten structure was used as the template molecule for each superposition. Superposition based on various molecular similarity measures produced qualitatively similar results.

Reported point charges are based on fitting to the computed electrostatic potential using the CHELPG scheme of Breneman.[18] Electrostatic potential surfaces for stationary points and haptens (Figures 6 and 7) were created using SPARTAN.[17] The electrostatic potential for each structure was mapped onto a total electron density surface contoured at 0.002 e/au^3. The scale of electrostatic potential displayed for each case is consistent, ranging from −146 kcal/mol (red) to −20 kcal/mol (blue).

Kinetic isotope effects (KIEs) were computed using the method of Bigeleisen and Mayer.[19] RHF/6-31+G(d) vibrational frequencies, scaled by 0.9153,[10] were used in the calculations, and tunneling corrections[19c] were included. KIEs were computed for reactions starting from both isolated *p*-nitrophenyl acetate **15** and ion−molecule complex **16**. Although results from both were reasonable, those using complex **16** were closer to experiment[3a] and are reported below.

Results and Discussion

Phenyl Acetate Hydrolysis. Previous computational studies examined the base-catalyzed hydrolyses of several alkyl esters at the PM3, Hartree−Fock, and MP2 levels and the base-catalyzed hydrolysis of phenyl acetate at the AM1 level. Ohkubo and co-workers reported a structure of the tetrahedral intermediate involved in methyl acetate hydrolysis derived from ab initio calculations using the STO-3G basis set,[20] and Teraishi and co-workers optimized geometries of tetrahedral intermediates (in various protonation states) involved in methyl acetate hydrolysis at the MP2/6-31+G(d) level.[21] Shields and co-workers optimized geometries of tetrahedral intermediates and transition states for the addition of hydroxide ion to methyl acetate and methyl benzoate using both semiempirical and ab initio methods.[22] Pranata reported a detailed study of the complete RHF/6-31+G(d) gas phase reaction pathway for the base-catalyzed hydrolysis of methyl formate,[23] and Hori carried out a similar study at the RHF/6-31+G level for the hydrolysis of methyl acetate.[24] Shields and Landry and co-workers also located transition state structures for the addition step in the hydrolysis of cocaine with the PM3 and SM3 methods.[25] In addition, Luzhkov and Venanzi reported AM1 calculations for the reaction of phenyl acetate and hydroxide ion in the gas phase and in solution, as well as analogous calculations on the reaction of phenyl acetate with cyclodextrin,[26] and related work by Lightstone and Bruice examined the intramolecular displacement of phenoxide ion from phenyl esters by carboxylate nucleophiles at the RHF/6-31+G(d) level.[27]

(a) Reactants and Products. Calculated enthalpic and entropic contributions to the relative free energies of all stationary points involved in phenyl acetate hydrolysis are shown in Tables 1 and 2. Gas phase geometries and CHELPG charges for reactants and products are shown in Figure 1. Phenyl acetate (**1**) and hydroxide ion (**2**) form an ion−molecule complex (**3**) in the gas phase. This complex is approximately 20 kcal/mol more stable than the isolated reactants (Table 1). Unlike the case of *N*-phenylacetamide,[28] and in contrast to earlier AM1 calculations on phenyl acetate,[29] no fully conjugated *Z* isomer of **1** could be located. In fact, the fully conjugated conformation corresponds to a transition state for phenyl rotation at the RHF/6-31+G(d) level. In complex **3**, the hydroxide oxygen is weakly hydrogen-bonded to one of the *ortho*-hydrogens on the phenyl ring (resulting in a slight lengthening of the *o*-C−H bond and localization of positive charge on this hydrogen relative to the other *ortho*-hydrogen [+0.25 versus +0.11]). The hydroxide ion is thus oriented for attack on the carbonyl at an angle of 114°.

A product complex (**4**) between phenoxide (**8**) and acetic acid (**9**) was also located (Figure 1). This complex is approximately 6−11 kcal/mol more stable than fully

(17) *SPARTAN V4.0*, 1995, Wavefunction, Inc., 18401 Von Karman Ave., #370, Irvine, CA 92715.
(18) Breneman, C. M.; Wiberg, K. B. *J. Comput. Chem.* **1990**, *11*, 361−373.
(19) (a) Saunders: M.; Laidig, K. E.; Wolfsberg, M. J. *J. Am. Chem. Soc.* **1989**, *111*, 8989−8994. (b) Bigeleisen, J.; Mayer, M. G. *J. Chem. Phys.* **1947**, *15*, 261−267. (c) Bell, R. P. *The Tunnel Effect in Chemistry*; Chapman and Hall: New York, 1980; pp 60−63.
(20) Ohkubo, K.; Urata, Y.; Seri, K.; Ishida, H.; Sagawa, T.; Nakashima, T.; Imagawa, Y. *J. Mol. Catal.* **1994**, *90*, 355−365.
(21) Teraishi, K.; Saito, M.; Fujii, I.; Nakamura, H. *Tetrahedron Lett.* **1992**, *33*, 7153−7156.
(22) (a) Sherer, E. C.; Turner, G. M.; Shields, G. C. *Int. J. Quantum Chem., Quantum Biol. Symp.* **1995**, *22*, 83−93. (b) Turner, G. M.; Sherer, E. C.; Shields, G. C. *Int. J. Quantum Chem., Quantum Biol. Symp.* **1995**, *22*, 103−112.
(23) Pranata, J. *J. Phys. Chem.* **1994**, *98*, 1180−1184.
(24) Hori, K. *J. Chem. Soc., Perkin Trans. 1* **1992**, 1629−1633.
(25) (a) Sherer, E. C.; Turner, G. M.; Lively, T. N.; Landry, D. W.; Shields, G. C. *J. Mol. Modeling* **1996**, *2*, 62−69. (b) Sherer, E. C.; Yang, G.; Turner, G. M.; Shields, G. C.; Landry, D. W. *J. Phys. Chem. A* **1997**, *101*, 8526−8529.
(26) Luzhkov, V. B.; Venanzi, C. A. *J. Phys. Chem.* **1995**, *99*, 2312−2323.
(27) Lightstone, F. C.; Bruice, T. C. *J. Am. Chem. Soc.* **1997**, *119*, 9103−9113.
(28) Manea, V. P.; Wilson, K. J.; Cable, J. R. *J. Am. Chem. Soc.* **1997**, *119*, 2033−2039.
(29) Lee, I.; Kim, C. K.; Lee, B.-S. *J. Chem. Res., Synop.* **1990**, 42−43.

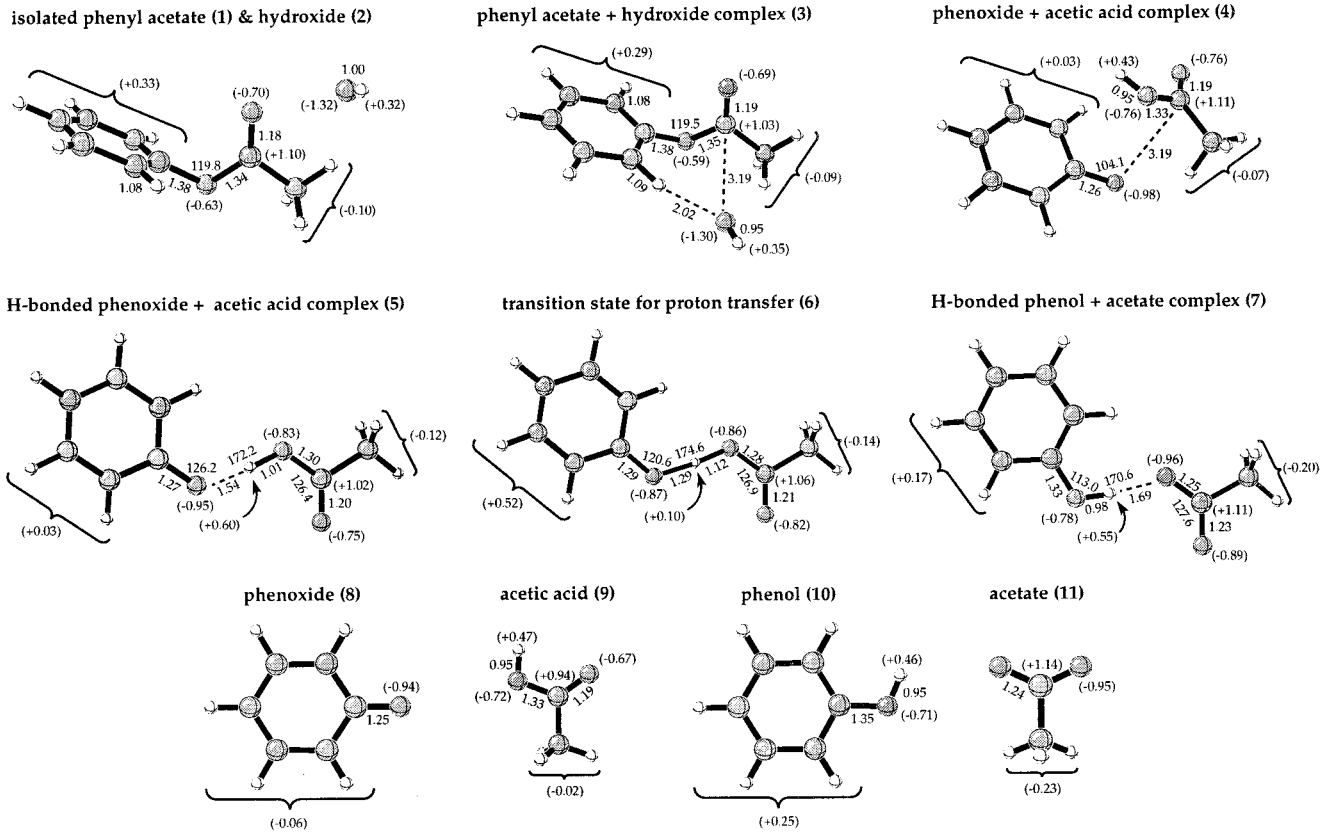

Figure 1. RHF/6-31+G(d) geometries and MP2/6-31+G(d) CHELPG charges (in parentheses) of starting materials and products. Distances are in angstroms and angles are in degrees.

dissociated **8** and **9** (Table 1). Geometries of the isolated and complexed **8** and **9** are nearly identical except that the O−H bond in **4** has rotated by approximately 19° out of the plane of the ester.

Other complexes of the hydrolysis products which involve strong hydrogen-bonding interactions were also examined (see Figure 1). Moving **8** and **9** into a hydrogen-bonded arrangement to produce planar complex **5** lowers their energy by approximately 13 kcal/mol below that of complex **4** (Table 1). A transition state (**6**) for proton transfer to form complex **7** was also located. When the energies of **5**, **6**, and **7** are adjusted to include corrections for zero point energy, however, the proton transfer process becomes barrierless (Table 1). This scenario is the hallmark of a short strong hydrogen bond (SSHB). MP2 single point calculations also predict that **6** is more stable than **5** or **7**. In light of the energy difference between **5** and **7** (approximately 6 kcal/mol), the actual structure of the hydrogen-bonded complex produced when **8** and **9** interact most likely resembles **7**. An analogous situation was observed for complexes involving the higher energy anti conformer of acetic acid.

AM1 calculations have been reported for the reaction of isolated phenyl acetate and hydroxide to produce isolated phenol and acetate ion.[26] These calculations predicted this transformation to be exothermic by approximately 68 kcal/mol,[26] while we calculate an exothermicity of 43−50 kcal/mol (Table 1). This smaller value is in much better agreement with the experimental gas phase value of 42.6 kcal/mol (derived from heats of formation).[30] The Langevin dipole solvent model was used along with the AM1 calculations to address solvation,[26] and this model predicted the hydrolysis reaction to be approximately 35−45 kcal/mol less exothermic in water than in the gas phase. Solvent cavity models, implemented here at the RHF/6-31+G(d) level, predict a smaller effect in which the stabilization of hydroxide ion is partly matched by the stabilization of isolated **10** and **11**; SCI-PCM calculations predict that the reaction is only 11 kcal/mol less exothermic in water, and PCM calculations suggest that it is approximately 30 kcal/mol less exothermic (see Table 1). For calibration, the solvation energy predicted for phenyl acetate by SCI-PCM is 6.6 kcal/mol, by PCM 11.0 kcal/mol, by AM1/LD(Q^C) 26.1 kcal/mol,[26] and by AM1/LD(Q^{PD}) 15.9 kcal/mol.[26] The reported experimental solvation energy is 12.7 kcal/mol,[31] suggesting that the AM1/LD calculations tend to overestimate the effects of aqueous solvation and that SCRF calculations tend to underestimate these effects. Despite the fact that discreet solvent−solute interactions are not treated explicitly by SCRF methods, PCM is reasonably close to experiment for this case, as it is for the case of hydroxide ion solvation (predicted solvation energy (PCM) = 113.4 kcal/mol, predicted solvation energy (SCI-PCM) = 70.3 kcal/mol, experimental solvation energy = 102.8 kcal/mol).[32] Considering the hydrolysis reaction to proceed from isolated **1** and **2** to hydrogen-bonded complex

(30) (a) Pedley, J. B.; Naylor, R. D.; Kirby, S. P. *Thermochemical Data of Organic Compounds*; Chapman and Hall: New York, 1986. (b) Chase, M. W., Jr.; Davies, C. A.; Downey, J. R., Jr.; Frurip, D. J.; McDonald, R. A.; Syverud, A. N. *J. Phys. Chem. Ref. Data, Suppl. 1* **1985**, *14*, 1−1856. (c) Cox, J. D. *Pure Appl. Chem.* **1961**, *2*, 125−128. (d) Wenthold, P. G.; Squires, R. R. *J. Am. Chem. Soc.* **1994**, *116*, 11890−11897.

(31) Wilson, B.; Georgiadis, R.; Bartmess, J. E. *J. Am. Chem. Soc.* **1991**, *113*, 1762−1766.

(32) Marcus, Y. *J. Chem. Soc., Faraday Trans.* **1991**, *87*, 2995−2999.

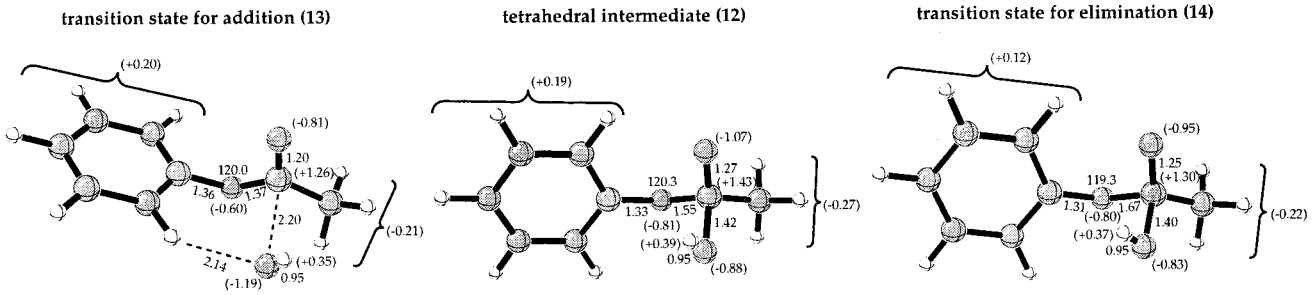

Figure 2. RHF/6-31+G(d) geometries and MP2/6-31+G(d) CHELPG charges (in parentheses) of tetrahedral intermediate **12** and transition states **13** and **14**. Distances are in angstroms and angles are in degrees.

7 results in a predicted exothermicity in the gas phase of 69.8−73.0 kcal/mol (Table 1), again in excellent agreement with the experimentally derived value of 68.7 kcal/mol.[30,33] In this case, solvation calculations predict that an aqueous environment will have a large effect, reducing the exothermicity to only 42.1 kcal/mol (by SCI-PCM) or 25.5 kcal/mol (by PCM, Table 1); hydrogen-bonded complex **7** is stabilized to a much lesser extent than isolated **10** and **11**, accentuating the differential stabilization of reactants and products in this case.

(b) Tetrahedral Intermediate. A tetrahedral intermediate (**12**) along the reaction pathway was also located (Figure 2). Compared to phenyl acetate (**1**), a slight shortening of the Ph−O bond (0.05 Å) and a lengthening of the PhO−C bond (0.21 Å) is observed for **12**, reflecting the tendency of the phenoxide leaving group to be expelled. The C−O^- bond is also lengthened (by 0.09 Å), but it is still substantially shorter than that of a simple alkoxide (cf. 1.33 Å for methoxide at the same level of theory). The Ph−O−C−Me dihedral angle is approximately 180°, as expected on the basis of stereoelectronic effects.[34] Alternative conformations about the PhO−C bond were examined, but only one conformer distinct from **12** (that with the phenyl group rotated by approximately −30°) could be located. This conformer was equienergetic with **12**. A transition state for phenyl rotation was located, but the calculated barrier to rotation is only 2 kcal/mol. In addition, transition states for rotation of the O−H bond and for racemization of the intermediate by direct proton transfer through a four-membered cycle were located. These transition states are approximately 10 and 30 kcal/mol higher in energy than **12**.

The geometry of **12** differs from the geometries of tetrahedral intermediates involved in methyl ester hydrolysis previously calculated at the RHF and MP2 levels.[20−24] These studies consistently predicted C−O^- bond lengths of approximately 1.30 Å, C−OH bond lengths of 1.43−1.50 Å, and MeO−C bond lengths of 1.44−1.52 Å for tetrahedral intermediates. The C−O^- and C−OH bond lengths calculated for the phenyl case are slightly shorter, and the PhO−C bond length is longer, than the analogous distances in the methyl cases, reflecting the difference in leaving group ability between phenoxide and methoxide ions. This is in contrast to a tetrahedral intermediate involved in intramolecular displacement of phenoxide ion by a carboxylate group described by Lightstone and Bruice.[27] In this case, the PhO−C bond is only 1.46 Å long while the C−O(carboxylate) bond is 1.55 Å long, consistent with the fact that the carboxylate moiety is a better leaving group than phenoxide ion.

(c) Transition States for Addition and Elimination. The structure of ion−molecule complex **3** is directly related to that of the transition state for hydroxide addition to the carbonyl carbon of phenyl acetate (**13**, Figure 2). The C−H···O hydrogen bond in **3** appears to recruit the hydroxide ion to the vicinity of the carbonyl and its π^* antibonding orbital. The overlap of the hydroxide lone pair electrons with this orbital then increases (the O- - -C distance decreases by almost an angstrom, the carbonyl bond lengthens slightly, and charge is redistributed from the hydroxide oxygen to the carbonyl oxygen). The angle of attack shifts from 114° in complex **3** to 106° in transition state **13**. The length of the forming bond (2.20 Å) is considerably shorter than that reported for hydroxide ion attack on methyl formate (3.28 Å),[23] reflecting the increased electrophilicity of aryl esters relative to their alkyl ester counterparts. IRC calculations on **13** confirm that this transition structure evolves toward complex **3** in one direction and toward tetrahedral intermediate **12** in the other.

Transition state **13** is calculated to be approximately 20 kcal/mol less stable than tetrahedral intermediate **12** (Table 1). Earlier AM1 calculations predicted that a tetrahedral intermediate would be approximately 50 kcal/mol lower in energy than the transition state for addition.[26] It is this difference in exothermicities which leads to the large discrepancy between AM1 and ab initio calculations in predicting the overall exothermicity for the hydrolysis reaction as noted above.

A transition state for expulsion of phenoxide (**14**) was also located (Figure 2). This structure is barely distorted from that of tetrahedral intermediate **12**. Shortening of the Ph−O bond (0.02 Å), the incipient carbonyl bond (0.02 Å), and the C−OH bond (0.02 Å), along with lengthening of the breaking PhO−C bond (0.12 Å), relative to **12** are indicative of the slight changes necessary to achieve the transition state for phenoxide expulsion. Analysis of the transition vector and IRC calculations verify that this is a transition state for PhO−C bond breaking.

The length of the breaking PhO−C bond (1.67 Å) is significantly shorter than distances reported for the breaking MeO−C bonds in transition states for loss of methoxide from methyl formate (1.90 Å at the RHF/6-31+G(d) level)[23] and methyl acetate (2.00 Å at the RHF/6-31+G level).[24] Methoxide expulsion is accompanied by proton transfer in these cases; the corresponding elimi-

(33) Meot-Ner, M.; Sieck, L. W. *J. Am. Chem. Soc.* **1986**, *108*, 7525−7529.

(34) Deslongchamps, P. *Stereoelectronic Effects in Organic Chemistry*; Pergamon Press: New York, 1983.

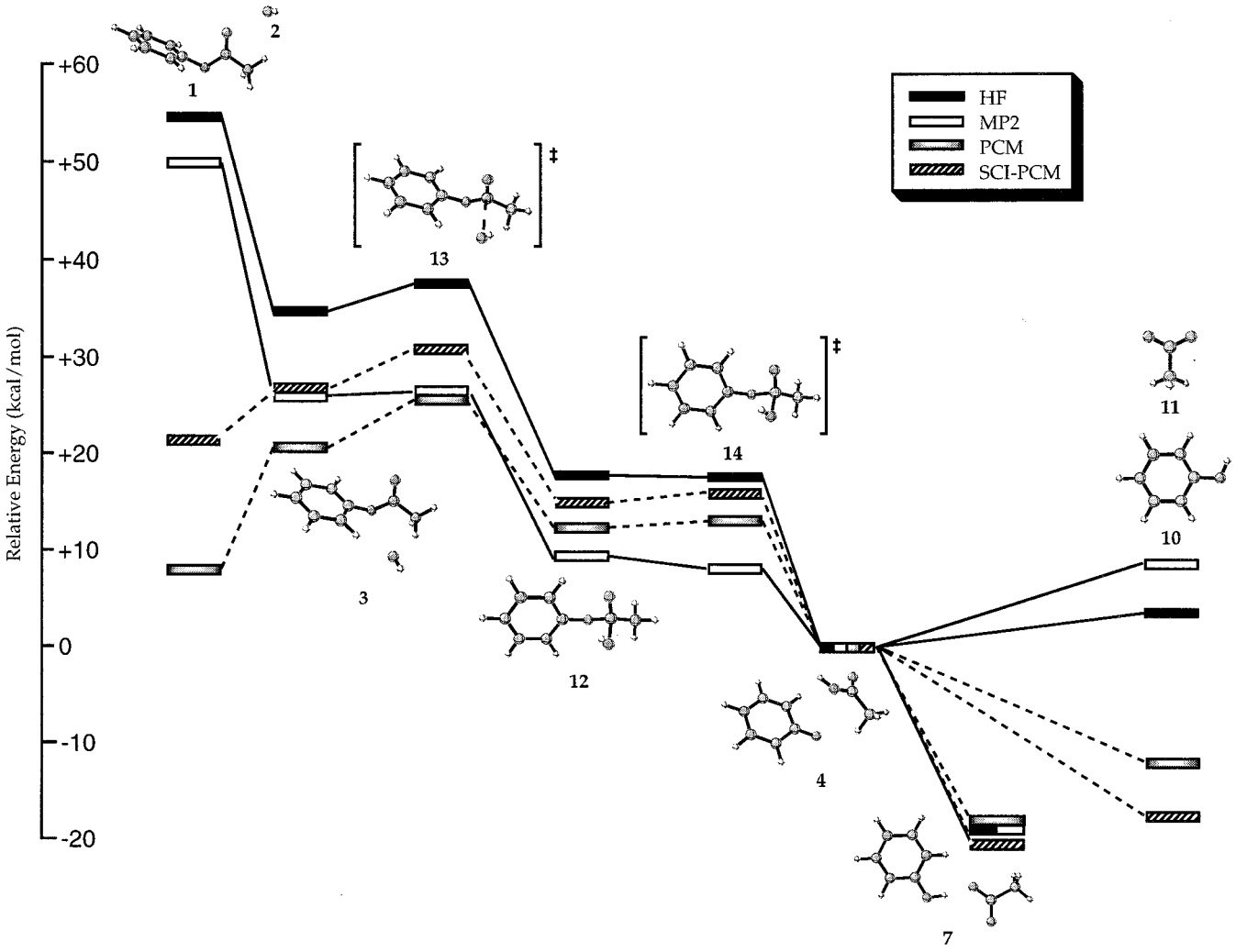

Figure 3. Reaction pathway for the stepwise hydrolysis of phenyl acetate. Enthalpies of RHF/6-31+G(d) stationary points calculated at various levels of theory are graphed relative to the enthalpy of complex **4**.

nation transition states exhibit weak hydrogen bonds (1.97 Å for methyl formate[23] and 1.93 Å for methyl acetate[24]) between the hydroxyl proton and the methoxide leaving group. This interaction stabilizes the relatively poor methoxide leaving group, and this is reflected in a late transition state. Such an interaction is not observed in the phenoxide case, due to the reduced basicity of the phenoxide oxygen.

(d) Overall Hydrolysis Pathway. The overall gas phase hydrolysis pathway is shown in Figure 3. Starting from isolated phenyl acetate **1** and hydroxide ion **2**, an intermediate complex **3** is formed exothermically (see also Table 1). This complex rearranges to tetrahedral intermediate **12** by passage through transition state **13**. This process has associated with it a very small barrier (0.5−3.3 kcal/mol not including the 2 kcal/mol entropy barrier calculated at 298 K, Tables 1 and 2). The tetrahedral intermediate (**12**) then rearranges to a product complex (**4**) which is 4−8 kcal/mol more stable than fully dissociated phenol **10** and acetate ion **11** but 19 kcal/mol less stable than hydrogen-bonded complex **7**. Phenoxide expulsion proceeds through transition state **14**, but the barrier associated with this transition state (0.2 kcal/mol) disappears when zero point energy corrections or electron correlation are included ($-T\Delta S$ is 0.2 kcal/mol at 298 K, too small to produce a positive free energy of activation, Table 2). This is in contrast to the barriers of 4−9 kcal/mol reported for the collapse of tetrahedral intermediates involved in the hydrolyses of methyl formate and methyl acetate.[21,23−24] Higher levels of theory are unlikely to locate tetrahedral intermediates and transition structures analogous to **12** and **14**. Therefore, the gas phase hydrolysis of phenyl acetate is concerted.

The effects of aqueous solvation have also been examined using PCM and SCI-PCM calculations as described above. The most significant effect of solvation is to lower the energy of unassociated reactants **1** and **2** below the energy of complex **3**, making this complex irrelevant in solution and increasing the barrier for addition to 10−20 kcal/mol, depending on the solvent cavity model used (see Table 1 and Figure 3). These predictions agree well with the experimental activation energy of 12.6 kcal/mol measured for phenyl acetate hydrolysis in aqueous acetone.[35] In addition, the barrier to the elimination step is predicted to be only 1−2 kcal/mol in solution, suggesting that a tetrahedral intermediate is formed but is extremely reactive toward phenoxide expulsion.

***p*-Nitrophenyl Acetate Hydrolysis.** The alkaline hydrolysis of *p*-nitrophenyl acetate was also examined.

(35) Tommila, E.; Hinshelwood, C. N. *J. Chem. Soc.* **1938**, 1801−1810.

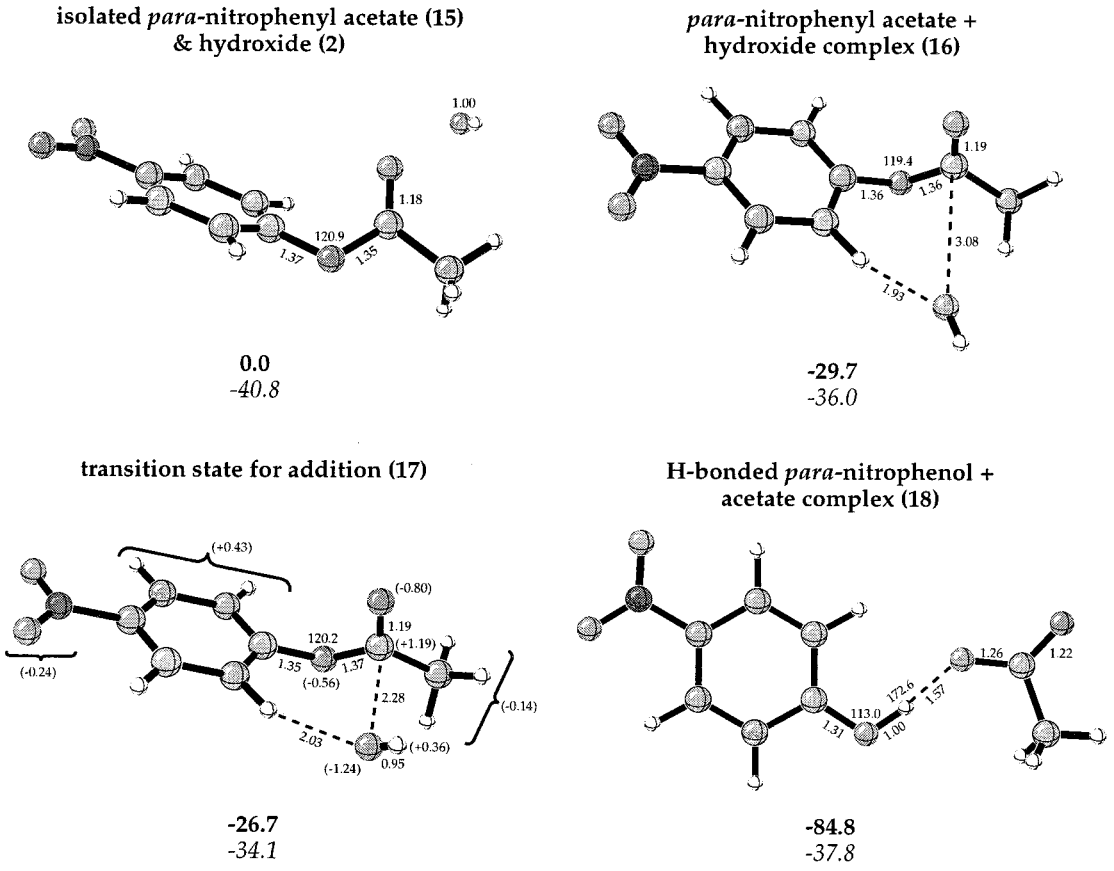

Figure 4. RHF/6-31+G(d) geometries, relative enthalpies (bold), and entropies ($-T\Delta S$, italic) of stationary points involved in *p*-nitrophenyl acetate hydrolysis. MP2/6-31+G(d) CHELPG charges (in parentheses) are shown for transition state **17**. Distances are in angstroms and angles are in degrees.

RHF/6-31+G(d) optimized structures, relative enthalpies and entropies of isolated *p*-nitrophenyl acetate **15** and hydroxide ion **2**, an ion−molecule complex between them (**16**), a transition state for hydroxide attack (**17**), and a hydrogen-bonded complex between *p*-nitrophenol and acetate ion (**18**) are shown in Figure 4. Efforts to locate a tetrahedral intermediate were unsuccessful even at the RHF level. Starting geometries were obtained by adding a *p*-nitro group to **12**. At the RHF/3-21G level, optimization led to a *p*-nitrophenoxide/acetic acid product complex. Optimizations at the RHF/6-31+G(d) level did not converge.

The structures of these stationary points are similar to those for phenyl acetate hydrolysis, although slight differences in bond lengths result from the presence of the nitro moiety (compare Figures 1, 2, and 4). For example, the largest differences between addition transition states **17** and **13** result from a strengthening of the C−H···O hydrogen-bonding interaction (the C−H···O distance is 2.03 Å for the *p*-nitrophenyl case compared to 2.14 Å for the phenyl case) due to the presence of the electron-withdrawing nitro group. This interaction is in competition with the interaction between the hydroxide lone pair electrons and the carbonyl π^* antibonding orbital, and a lengthening of the hydroxide−carbonyl distance (0.08 Å) is consequently observed, although the angle of attack is unaffected. The small barrier associated with this transition state is only slightly less than that associated with **13** (compare Figure 4 and Tables 1 and 2). Attempts to locate a transition state analogous to **14** were also unsuccessful. This is not surprising in light of the instability of tetrahedral intermediate **12** and the fact that the addition of a nitro moiety produces a superior leaving group. These results are consistent with a concerted hydrolysis process in the gas phase, the overall exothermicity of which is approximately 12 kcal/mol greater than that of the phenyl case (compare Figure 4 and Tables 1 and 2). SCI-PCM solvation calculations predict a barrier of 6.2 kcal/mol for the concerted process, a value which is approximately 4 kcal/mol lower than that for phenyl acetate hydrolysis (a lowering of 1.6 kcal/mol is measured experimentally).[35]

Isotopic labeling studies have also suggested that attack of hydroxide ion on *p*-nitrophenyl acetate is a concerted process,[3a] and our calculations are consistent with these results as well. Computations predict kinetic isotope effects (KIEs) slightly greater than 1.00 for $^{14}N/^{15}N$ (nitro group), $^{16}O/^{18}O$ (phenolic oxygen), and $^{16}O/^{18}O$ (carbonyl oxygen), and a KIE of approximately 0.95 for H/D (trideuterated methyl group); such KIEs are observed experimentally (see Table 3).[3a]

Comparisons with Haptens: Geometries, Charges, and Electrostatic Potential Surfaces. The structures of the stationary points involved in aryl acetate hydrolysis described above were compared with those of the haptens used to elicit various hydrolytic antibodies. Hydrolytic antibodies 48G7, CNJ206, and 17E8 have been characterized by X-ray crystallography.[13−15] The haptens used to elicit these antibodies, along with the substrates whose hydrolyses they catalyze, are shown in Table 4. Biochemical and structural evidence suggests that at basic pHs antibodies 48G7 and CNJ206 function

Table 3. Experimental and Calculated (RHF/6-31+G(d)) Intramolecular Kinetic Isotope Effects for Attack of Hydroxide Ion on *p*-Nitrophenyl Acetate

isotopomer	$^{14/15}$N (NO_2)	$^{16/18}$O (PhO)	$^{16/18}$O (C=O)	3H/D (Me)
exptl[3a]	1.0002	1.0135	1.0039	0.9562
calcd[a]	1.0004 (1.0004)	1.0006 (1.0007)	1.0079 (1.0081)	0.9505 (0.9510)

[a] Values in parentheses are corrected for tunneling.[19]

Table 4. Several Antibodies Which Catalyze the Hydrolysis of Aryl Esters

antibody	hapten	substrate	k_{cat}/k_{uncat}
48G7	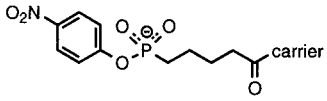	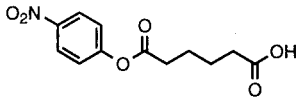	1.6×10^4
CNJ206	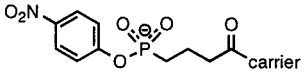	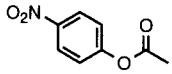	1.6×10^3
17E8	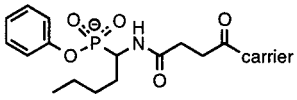	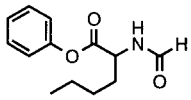	8.3×10^3

[a] See ref 39 and references therein.

in accord with the mechanism programmed by their haptens: displacement of the aryloxide leaving group of the ester by hydroxide.[36−39] It has been suggested that antibody 17E8 may achieve catalysis through a mechanism involving an acyl−antibody intermediate, but a related antibody, 29G11, which was produced in the same immunization, is highly homologous to 17E8 and appears to utilize the same mode of catalysis as 48G7 and CNJ206.[38−40]

Several previous computational studies examined the structures of TSAs and compared them with various tetrahedral intermediates and transition states. Teraishi and co-workers reported comparisons of MP2/6-31+G(d) structures of tetrahedral intermediates and phosphonate TSAs involved in methyl acetate hydrolysis,[21] and a similar study was reported by Ohkubo and co-workers at a lower level of theory (ab initio calculations with the STO-3G basis set).[20] Shields and co-workers compared ab initio calculated geometries for addition transition states and tetrahedral intermediates involved in the hydrolysis of methyl acetate and methyl benzoate with those of phosphonate haptens.[22] Shields, Landry, and co-workers also compared the PM3 and SM3 calculated geometries and electrostatic potential surfaces of transition states for hydroxide addition to cocaine with phosphonate and thiophosphonate TSAs designed to mimic them.[25] Various TSAs which function as inhibitors of a β-lactamase were examined by Curley and Pratt using force field calculations,[41] and TSA inhibitors of various proteases were examined by Houk and co-workers using ab initio calculations of conformations and analyses of electrostatic potential surfaces.[42] Overall, these studies suggest that alkyl phosphonates are reasonable mimics of tetrahedral intermediates involved in alkyl ester hydrolysis, although some differences in geometries and charge distributions have been noted.[21−22,25]

Several related studies also attempted to correlate various properties of substrates and tetrahedral intermediates with their free energy of binding to catalytic antibodies. Kodaka and Hase examined relationships between solvent accessible surface areas, enthalpies of hydration, polarizabilities, and dipole moments of substrates and tetrahedral intermediates (calculated with AM1) and their corresponding free energies of binding to various hydrolytic antibodies,[43] and Kollman and co-workers examined the binding of several substrates to antibody 17E8 using free energy perturbation calculations.[44]

Antibodies 48G7, CNJ206, and 17E8 catalyze the hydrolysis of aryl (rather than alkyl) esters, however, and our studies show that the tetrahedral intermediates involved in these reactions are unlikely to be stable and, in any case, are much lower in energy than rate-determining addition transition states. Since these transition state structures differ from those of tetrahedral intermediates, direct comparisons of actual aryl-substituted haptens with aryl-substituted transition states are necessary. Coordinates for the aryl phosphonate haptens used to elicit antibodies 48G7, CNJ206, and 17E8 were extracted from the coordinates of the corresponding hapten-bound X-ray structures deposited in the Protein Data Bank.[13−15] Antibodies 48G7 and CNJ206 were elicited in response to *p*-nitrophenyl phosphonate TSAs,

(36) Stevens, R. C.; Hsieh-Wilson, L. C.; Santatsiero, B. D.; Wedemayer, G. J.; Spiller, B.; Wang, L. H.; Barnes, D.; Ulrich, H. D.; Patten, P. A.; Romesberg, F. E.; Schultz, P. G. *Israel J. Chem.* **1996**, *36*, 121−132.
(37) Charbonnier, J.-B.; Golinelli-Pimpaneau, B.; Gigant, B.; Green, B. S.; Knossow, M. *Israel J. Chem.* **1996**, *36*, 143−149.
(38) Charbonnier, J.-B.; Golinelli-Pimpaneau, B.; Gigant, B.; Tawfik, D. S.; Chap, R.; Schindler, D. G.; Kim, S.-H.; Green, B. S.; Eshhar, Z.; Knossow, M. *Science* **1997**, *275*, 1140−1142.
(39) Macbeath, G.; Hilvert, D. *Chem. Biol.* **1996**, *3*, 433−445.
(40) Guo, J.; Huang, W.; Scanlan, T. S. *J. Am. Chem. Soc.* **1994**, *116*, 6062−6069. (b) Guo, J.; Huang, W.; Zhou, G. W.; Fletterick, R. J.; Scanlan, T. S. *Proc. Natl. Acad. Sci. U.S.A.* **1995**, *92*, 1694−1698.
(41) Curley, K.; Pratt, R. F. *J. Am. Chem. Soc.* **1997**, *119*, 1529−1538.
(42) Radkiewicz, J. L.; McAllister, M.; Goldstein, E.; Houk, K. N. *J. Org. Chem.* **1998**, *63*, 1419−1428.
(43) Kodaka, M.; Hase, A. *Bull. Chem. Soc. Jpn.* **1996**, *69*, 3571−3574.
(44) Fox, T.; Scanlan, T. S.; Kollman, P. A. *J. Am. Chem. Soc.* **1997**, *119*, 11571−11577.

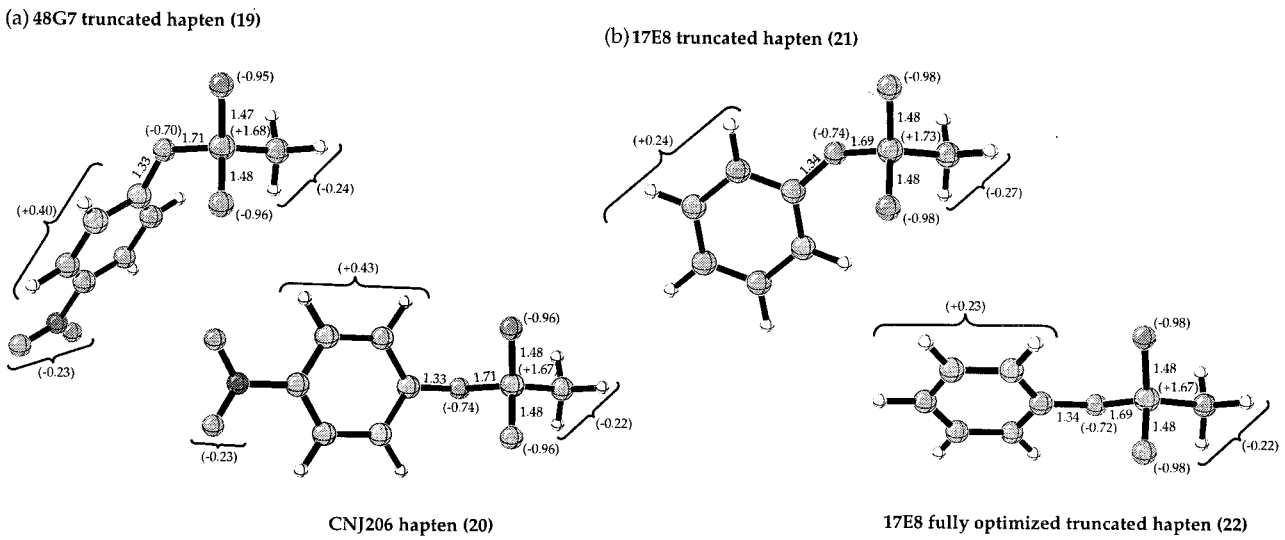

Figure 5. (a) Geometries of *p*-nitrophenyl phosphonate haptens used to elicit antibodies 48G7 and CNJ206 after constrained optimization. (b) Geometries of the hapten used to elicit antibody 17E8 after constrained and unconstrained optimization. Selected distances (Å), angles (deg), and CHELPG charges (in parentheses) are shown.

and 17E8 was elicited in response to a phenyl phosphonate hapten (Table 4). For the sake of comparison, the linker portion of each hapten was truncated to a methyl group, and geometries were optimized at the RHF/6-31+G(d) level with their torsional angles fixed to the X-ray values throughout the minimization procedure (**19**−**21**, Figure 5, see Methods section for details). MP2/6-31+G(d) single point calculations were performed on the resulting structures to obtain relative energies and CHELPG charges (Figure 5). Figure 5a shows the results for the *p*-nitrophenyl phosphonates from antibodies 48G7 and CNJ206. It appears that antibody CNJ206 binds its hapten in a conformation which (in the gas phase) is preferred over that found in antibody 48G7 by approximately 1 kcal/mol (at both the RHF and MP2 levels). Figure 5b shows the result of the constrained optimization of the 17E8 hapten, along with the result of an unconstrained RHF/6-31+G(d) geometry optimization (**22**). The unconstrained optimization leads to a relaxed structure that is approximately 2 kcal/mol more stable than that found in the X-ray structure (at both the RHF and MP2 levels). In both Figures 5a and 5b, the more stable conformer corresponds to the one which has the staggered backbone orientation found for the tetrahedral intermediates and transition states described above, but the small magnitude of the energy differences between these conformers suggests that the conformation in which the haptens bind is likely to have little or no effect on catalysis.

The central issue in this study, however, is how faithfully these haptens mimic transition states for hydrolysis. Geometrically, the haptens appear most similar to the elimination transition state **14** and tetrahedral intermediate **12** in terms of molecular volumes, bond lengths, and bond angles (compare Figures 2 and 5). They are less similar to addition transition state **13** and do not resemble reactant complex **3** or product complex **6**. Although the molecular volumes of **3**, **13**, **12**, **14**, and **6** are similar in magnitude to that of the truncated 17E8 hapten, the volume which each of these stationary points shares with this hapten when the two are superposed varies (see Methods section). **14** and **12** share the most volume with the hapten (approximately 92 and 93%, respectively), while **13**, **6**, and **3** share considerably less (85, 84, and 82%, respectively). Moreover, the P−O bond distances in the haptens do not mimic the C−O$^-$ and C−OH bond distances in the tetrahedral intermediate or transition states very closely. The haptens have distances between 1.47 and 1.48 Å for both P−O bonds. Transition state **13** has distances of 1.20 and 2.20 Å, tetrahedral intermediate **12** has distances of 1.27 and 1.42 Å, and transition state **14** has distances of 1.25 and 1.40 Å, for the C−O$^-$ and C−OH bonds, respectively. These values differ from those of the haptens in both magnitude and degree of bond length equalization, especially for addition transition state **13**. The distance between the two most negatively charged oxygens of the haptens and the corresponding distance in each of **12**−**14** provides a measure of the relative positions of two of the most important recognition elements in these molecules. This distance averages 2.40 Å for the haptens; it is 2.77 Å for **13**, 2.24 Å for **12**, and 2.23 Å for **14**. Again, the haptens seem to mimic transition state **13** less effectively than they mimic **12** and **14**. Despite the fact that **13** is less similar to the haptens than are **12** and **14**, all three can be selectively stabilized over reactants and products by an antibody that effectively binds hapten—exactly the situation required for catalysis. However, catalysis as programmed by the phosphonate haptens is most likely less effective than it would be if they selectively mimicked **13**, the transition state for the rate-determining addition step.

Comparison of electrostatic potential surfaces[45] for haptens and stationary points reveals additional sources of infidelity. Figures 6 and 7 show calculated electrostatic potential surfaces for stationary points **3**, **13**, **12**, **14**, and **4** (Figure 6) and hapten structures **20** and **22** (Figure 7). The electrostatic potential at each point on a constant electron density surface (which approximates the van der Waals surface for each structure) is represented graphically by a range of colors, with red corresponding to the regions where the electrostatic potential is most negative and blue corresponding to the least negative regions. The

(45) (a) Bagdassarian, C. K.; Schramm, V. L.; Schwartz, S. D. *J. Am. Chem. Soc.* **1996**, *118*, 8825−8836. (b) Schramm, V. I.; Horenstein, B. A.; Kline, P. C. *J. Biol. Chem.* **1994**, *269*, 18259−18262.

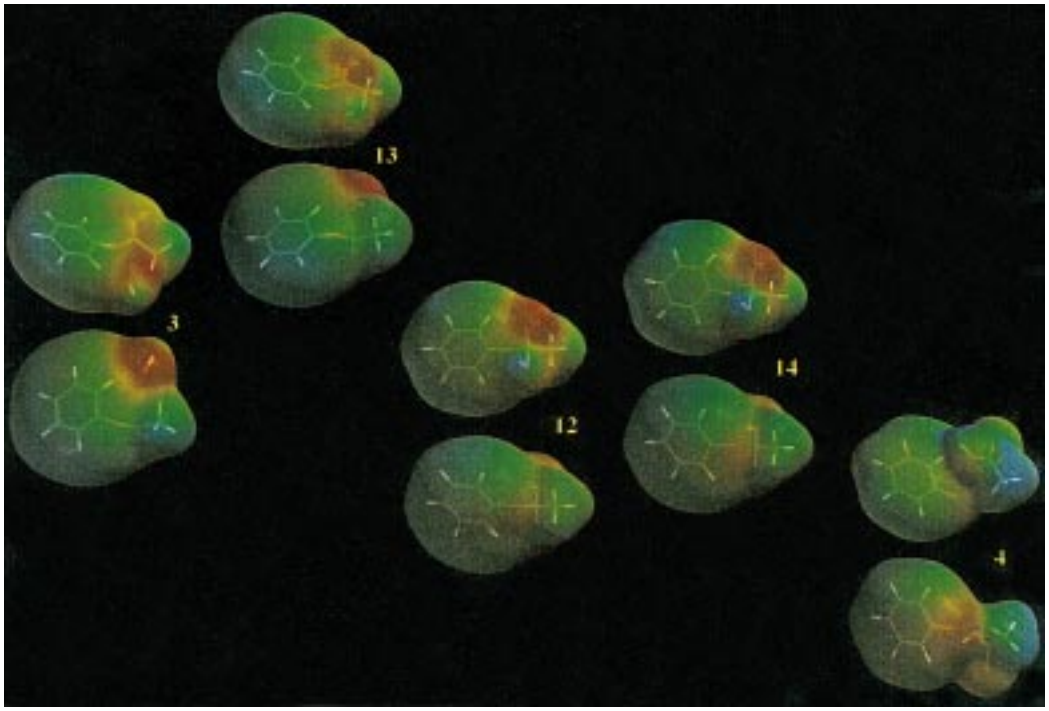

Figure 6. Electrostatic potential surfaces for stationary points involved in phenyl acetate hydrolysis. The lower structure of each pair corresponds to a view of its counterpart rotated by approximately 180° (around a horizontal axis passing through the molecule). Red areas indicate the most negative regions (see Methods section for details).

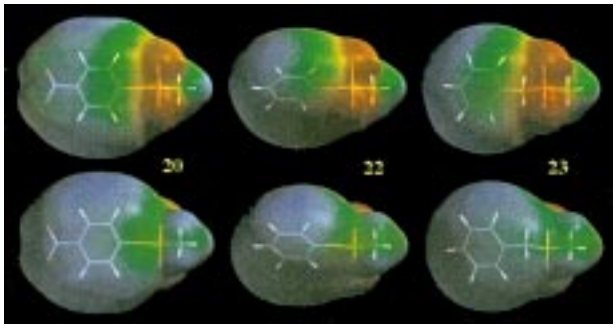

Figure 7. Electrostatic potential surfaces for hapten structures **20**, **22**, and **23**. The lower structure of each pair corresponds to a view of its counterpart rotated by approximately 180° (around a horizontal axis passing through the molecule). Red areas indicate the most negative regions (see Methods section for details).

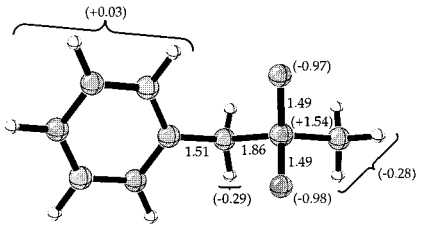

Figure 8. RHF/6-31+G(d) geometry and MP2/6-31+G(d) CHELPG charges (in parentheses) of phosphinate TSA **23**. Distances are in angstroms and angles are in degrees.

electrostatic recognition pattern presented by **13**, **12**, and **14** is significantly different than that presented by the haptens which elicited antibodies 48G7, CNJ206, and 17E8. A much larger concentration of negative charge is found around the oxygen atoms in the phosphonate structures (Figure 7) than around the corresponding atoms in **12**−**14** (Figure 6). This discrepancy is due in part to the substitution of a phosphorus atom in the analogs for a carbon atom in the actual intermediate and transition states, but the primary source of this infidelity is the presence of a proton on one of the oxygens in each of **13**, **12**, and **14**.

There are interesting implications of the geometric and electrostatic similarities and differences between **19**−**22** and **12**−**14**. Although the phosphonate haptens appear to be reasonably isosteric with the transition states and tetrahedral intermediates involved in hydrolysis, these haptens tend to overestimate most key C−O bond lengths; the one exception is the underestimation of the forming C−O bond in addition transition state **13**. Equally tight binding of the haptens, the intermediate, and the transition states is therefore unlikely. In terms of electrostatic properties, the phosphonate groups display a region of negative potential around their oxygen atoms which is considerably more intense than that around the corresponding atoms of **12**−**14** (TSAs based on the phosphinate group offer no significant improvement in geometrical or electrostatic mimicry of **12**−**14**; see **23** in Figures 7 and 8). This can both help and hurt catalysis. It is desirable to have a group in the active site to stabilize the developing negative charge on the carbonyl oxygen (an oxyanion hole), but it is undesirable, in terms of hydrogen bonding, to have such a group in the vicinity of the hydroxyl proton of **12**−**14**. The stability of this proton throughout the hydrolysis reaction makes it desirable to have a hydrogen-bond acceptor present on its side of the active site rather than a hydrogen-bond donor or cation.

Moreover, examination of the CHELPG charges shown in Figures 1 and 2 and the electrostatic potential surfaces shown in Figure 6 reveals a flow of negative charge from one side of the reacting complex to the other during hydrolysis. In particular, the attacking oxygen atom steadily becomes less negative and the carbonyl oxygen

becomes more negative throughout the rate-determining addition step. This implies that catalysis could be promoted by a dipolar arrangement of active site residues. However, the X-ray structures of antibodies 48G7, CNJ206, and 17E8 reveal that both the pro-*R* and pro-*S* phosphonate oxygens of the haptens are stabilized through salt bridges and hydrogen-bonding interactions with the side chains of combining site residues such as arginine, lysine, histidine, and tyrosine, as well as with backbone NH groups.[13−15,38−39] This is to be expected on the basis of the nature of the haptens, but likely does not provide the ideal arrangement of residues for catalysis. In fact, recent studies by Knossow and co-workers on antibody CNJ206 have suggested that although His H35 forms a hydrogen bond to a phosphonate oxygen in the hapten-bound crystal structure,[46] this residue is not directly involved in catalysis.[37] Mutagenesis of an active site hydrogen-bond donor or cationic residue to an aspartate or glutamate will create a dipolar binding site and may improve catalysis—providing that such a substitution can be made without disrupting the initial binding of reactants. Computations on the binding properties of such theoretical mutants are underway, and we are currently examining the geometric and electrostatic properties of asymmetric haptens designed to elicit antibodies with this alternative hydrogen-bonding pattern.

Conclusions

The alkaline hydrolysis reactions of both phenyl and *p*-nitrophenyl acetate are computed to be highly exothermic and concerted in the gas phase, in accord with experimental measurements. Solution calculations using solvent cavity models accurately reproduce the overall thermodynamics and activation barrier for alkaline hydrolysis of phenyl acetate in water. These calculations are consistent with formation of a tetrahedral intermediate in a very shallow minimum for the aqueous hydrolysis of phenyl acetate and a concerted pathway for the aqueous hydrolysis of *p*-nitrophenyl acetate. Comparisons between the structures of the transition states and intermediates involved in hydrolysis and the analogs designed to mimic them has revealed that although aryl phosphonates mimic some of the geometric features of the transition states and intermediates, they less effectively mimic the asymmetry and electrostatic properties of these stationary points. In particular, the haptens are much better analogues of tetrahedral intermediate **12** and elimination transition state **14** than they are of rate-limiting addition transition state **13**.

Acknowledgment. We are grateful to the National Science Foundation and the National Institutes of Health (Chemistry−Biology Interface Training Program fellowship to D.J.T.) for financial support of this research. We gratefully acknowledge grants of computer time from the UCLA Office of Academic Computing and the National Computational Science Alliance (under grant MCA93S015N, utilizing the NCSA SGI/CRAY POWER CHALLENGEarray and the NCSA HP-Convex Exemplar SPP-2000).

JO982335T

(46) Charbonnier, J. B.; Carpenter, E.; Gigant, B.; Golinelli-Pimpaneau, B.; Eshhar, Z.; Green, B. S.; Knossow, M. *Proc. Nat. Acad. Sci. U.S.A.* **1995**, *92*, 11721−11725.